

## Enhancing magnetic dipole emission in Eu-doped SrMO<sub>3</sub> ( $M = \text{Ti, Zr, Hf}$ ): First-principles calculations

Mu Lan<sup>1,2</sup>, Rong Wang<sup>3</sup>, Zeng-Hui Yang<sup>1,2</sup>, Xiaofeng Wang<sup>1,2</sup>, Song Sun<sup>1,2</sup> and Su-Huai Wei<sup>4,\*</sup>

<sup>1</sup>Microsystem and Terahertz Research Center, China Academy of Engineering Physics, 610200 Chengdu, China

<sup>2</sup>Institute of Electronic Engineering, China Academy of Engineering Physics, 621900 Mianyang, China

<sup>3</sup>Hangzhou Global Scientific and Technological Innovation Center, Zhejiang University, 311200 Hangzhou, China

<sup>4</sup>Beijing Computational Science Research Center, 100193 Beijing, China



(Received 5 January 2021; revised 13 April 2021; accepted 19 May 2021; published 8 June 2021)

Magnetic dipole (MD) spontaneous emission plays a vital role in the field of optical magnetism, which has been observed in trivalent lanthanide ions. In this case, the luminescence properties of the MD are largely affected by the crystal field symmetry at the embedding trivalent lanthanide ion site, but the correlation between the doping properties and the MD emission has not been fully understood. Here, we systematically investigate the doping properties of Eu in SrMO<sub>3</sub> ( $M = \text{Ti, Zr, Hf}$ ) using first-principles calculations, in order to maximize the MD emission efficiency of the Eu-doped perovskites. By analyzing the formation energies under the accessible growth conditions, we determine the ideal conditions for Eu-doped perovskites that could maximize the MD emission. We also theoretically demonstrate the spin flipping emission mechanism of Eu<sup>3+</sup>. Our study thus provides a guideline for the design of highly efficient MD emission materials.

DOI: [10.1103/PhysRevB.103.245201](https://doi.org/10.1103/PhysRevB.103.245201)

### I. INTRODUCTION

Spontaneous light emission is the foundation for a broad range of applications in both classic and quantum optics, such as the light-emitting device, sensing and imaging, and the single photon source among the others [1–3]. During the past decades, spontaneous electric dipole (ED) induced emission has been the mainstream research since the majority of the emitters (e.g., fluorescence dyes, quantum dots, etc.) are ED transition in nature. On the other hand, for a long time, magnetic dipole (MD) transition is believed to be unimportant because its emission strength is typically several orders of magnitude weaker than that of ED transition at optical frequency [4]. This perspective has been overthrown since the discovery of emission induced by rare earth trivalent lanthanide ions [5,6], which are proven to possess a strong MD transition that is comparable to the ED transition [7–10]. Recent development of optically induced magnetism has further rekindled the research interest on the MD-induced emission owing to its unique capability to interact with the optical magnetic field at the atomic level [11–13], whereas the ED can only interact with the optical electric field. However, the origin of the spontaneous MD-induced emission is not clear and, more importantly, it is not clear how to effectively control the MD transitions.

Among various trivalent lanthanide ions, europium ion (Eu<sup>3+</sup>) complexes are the most common materials for studying luminescence property in the visible light regime. The characteristic MD emission and the adjacent ED emission of Eu<sup>3+</sup> are at 592 and 612 nm, respectively, corresponding to the intra-atomic  $f$ - $f$  electronic transitions of  ${}^5D_0 \rightarrow {}^7F_1$  and

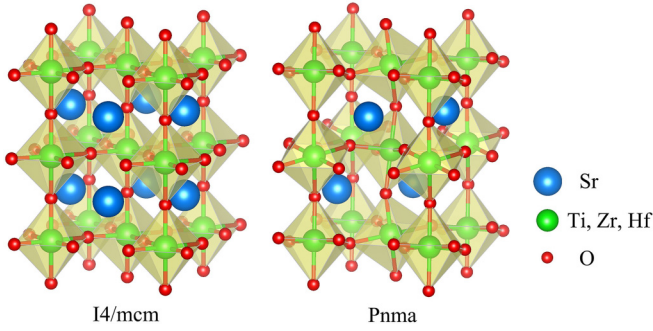
${}^5D_0 \rightarrow {}^7F_2$  [14]. Because of the localized nature of the  $f$  electrons, the chemical environment has little influence on Eu<sup>3+</sup> transition energies. However, its luminescence properties such as the intensity are largely impacted by the crystal field symmetry at the Eu<sup>3+</sup> site when it is embedded in some lattices because of the transition selection rules. For example, the intensity of  ${}^5D_0 \rightarrow {}^7F_1$  MD emission is strong only when Eu<sup>3+</sup> occupies an inversion site, while the  ${}^5D_0 \rightarrow {}^7F_2$  ED transition dominates when Eu<sup>3+</sup> occupies a noninversion site [15]. This rule has been widely used to determine the ratio between Eu on inversion and noninversion sites in host materials. Thus, to maximize the MD emission of a material doped with Eu, one should optimize the doping condition such that Eu<sup>3+</sup> atoms occupy inversion symmetry sites as much as possible. This requires that the host material has inversion centers as well as a large band gap to allow the excitation and emission from the luminescence center. It is noticed that some ABO<sub>3</sub> perovskites fulfill these conditions as candidate host materials for MD emission of Eu<sup>3+</sup>, but clear MD emission of these materials has yet to be elucidated [16–20].

In this work, we systematically investigate the Eu doping properties in SrMO<sub>3</sub> ( $M = \text{Ti, Zr, Hf}$ ) perovskites and develop strategy for maximizing MD emissions. Using first-principle calculations, we determine the accessible values of the chemical potential range of each element for thermodynamic equilibrium doping, and identify the ideal growth condition for the perovskites to maximize the Eu occupation at the  $M$  site as Eu<sub>M</sub>(−1) for MD emission applications.

### II. METHODS

Spin-polarized first-principle calculations are performed within the density functional theory (DFT) framework, as implemented in the Vienna *ab initio* simulation package

\*suhuaiwei@csrc.ac.cn

FIG. 1. Perovskite structures of  $I4/mcm$  phase and  $Pnma$  phase.

(VASP) [21] with the projector augmented wave (PAW) pseudopotentials [22]. The exchange and correlation interaction between electrons are described with the strongly constrained and appropriately normed semilocal density functional (SCAN) meta generalized gradient approximation (metaGGA) [23,24]. Semicore electrons are explicitly treated for Sr( $4s^2 4p^6 5s^2$ ), Ti( $3s^2 3p^6 4s^2 3d^2$ ), Zr( $4s^2 4p^6 5s^2 4d^2$ ), Hf( $5s^2 5p^6 6s^2 5d^2$ ), Eu( $5s^2 5p^6 6s^2 4f^7$ ), and O( $2s^2 2p^4$ ). The kinetic-energy cutoff is set to 520 eV. Electronic energy minimization is performed with a tolerance of  $10^{-7}$  eV, while the force on each atom is converged within 0.03 eV/Å. All the calculations are performed with a large supercell of 160 atoms. Because of large dielectric constants of SrTiO<sub>3</sub>, SrZrO<sub>3</sub>, and SrHfO<sub>3</sub>, the charge corrections are expected to be smaller than 0.01 eV with charge of  $\pm 1$ . For simplicity, the charge correction is not included in our calculation. Because the SCAN exchange and correlation potential underestimates the band gap, we use the HSE06 hybrid functional with 25% nonlocal Hartree-Fock exchange to calculate the band gaps of perovskites [25]. The calculated emission energy of Eu is in good agreement with experiments. We find that for SrZrO<sub>3</sub> and SrHfO<sub>3</sub>, the most stable phase is the orthorhombic phase (space group  $Pnma$ ). Although cubic phase (space group  $Pm-3m$ ) is stable for SrTiO<sub>3</sub> at room temperature, the tetragonal phase (space group  $I4/mcm$ ) is observed when doped with Eu at room temperature [26–28]. So, we consider the tetragonal phase for SrTiO<sub>3</sub> in the following study. These structures are shown in Fig. 1.

### III. RESULTS AND DISCUSSION

At first, we compare the lattice parameters and band gaps of SrTiO<sub>3</sub>, SrZrO<sub>3</sub>, and SrHfO<sub>3</sub> calculated with PBE, SCAN, and HSE06 functionals. In Tables I and II, we could notice that the SCAN functional can give a better description of lattice parameters and band gaps than PBE results. Despite

TABLE I. Lattice parameters and band gaps of SrTiO<sub>3</sub>, SrZrO<sub>3</sub>, and SrHfO<sub>3</sub> calculated with PBE, SCAN, and HSE06 functionals. Lattice parameters of SrTiO<sub>3</sub>, SrZrO<sub>3</sub>, and SrHfO<sub>3</sub> (unit: Å).

	PBE	SCAN	Experimental
SrTiO <sub>3</sub>	$a = 5.568, c = 7.907$	$a = 5.516, c = 7.834$	$a = 5.511, c = 7.796$ [29]
SrZrO <sub>3</sub>	$a = 5.847, b = 5.912, c = 8.298$	$a = 5.790, b = 5.836, c = 8.209$	$a = 5.791, b = 5.811, c = 8.196$ [30]
SrHfO <sub>3</sub>	$a = 5.800, b = 5.832, c = 8.213$	$a = 5.750, b = 5.768, c = 8.138$	$a = 5.752, b = 5.765, c = 8.134$ [31]

TABLE II. Band gaps of SrTiO<sub>3</sub>, SrZrO<sub>3</sub>, and SrHfO<sub>3</sub> (unit: eV) (HSE06 band gap calculations are based on the SCAN optimized lattices).

	PBE	SCAN	HSE06	Experimental
SrTiO <sub>3</sub>	1.858	2.273	3.379	3.25 [32]
SrZrO <sub>3</sub>	3.626	4.279	5.332	5.6 [33]
SrHfO <sub>3</sub>	4.177	4.735	5.808	6.1 [34]

higher accuracy on the band gaps, the HSE06 calculations of Eu-doped perovskites are computationally costly. So, we will use SCAN functional in the following discussion.

In these distorted perovskites, the doping configurations of Eu in the perovskites include substitution on the Sr site (Eu<sub>Sr</sub>), substitution on the  $M$  site (Eu<sub>M</sub>), and on the interstitial site (Eu<sub>i</sub>) [35,36]. Only the Eu<sub>M</sub> site has inversion symmetry as the center of the  $MO_6$  octahedral. Therefore, Eu<sub>M</sub> rather than Eu<sub>i</sub> or Eu<sub>Sr</sub> are preferred for maximizing the MD emission. The formation energies of doped Eu can be calculated as a function of atomic chemical potentials and the electron Fermi level [37]:

$$\Delta H_f(\alpha, q) = \Delta E(\alpha, q) + n_{\text{Sr}}\mu_{\text{Sr}} + n_{\text{M}}\mu_{\text{M}} + n_{\text{Eu}}\mu_{\text{Eu}} + qE_F, \quad (1)$$

where

$$\Delta E(\alpha, q) = E(\alpha, q) - E(\text{SrMO}_3) + n_{\text{Sr}}E(\text{Sr}) + n_{\text{M}}E(\text{M}) + n_{\text{Eu}}E(\text{Eu}) + qE_{\text{VBM}},$$

$E_F$  is the Fermi level referenced to the valence band maximum (VBM) of SrMO<sub>3</sub>.  $\mu_{\text{Sr}}$ ,  $\mu_{\text{M}}$ , and  $\mu_{\text{Eu}}$  are the chemical potentials of Sr,  $M$ , and Eu referenced to their elemental solids with energies of  $E(\text{Sr})$ ,  $E(\text{M})$  and  $E(\text{Eu})$ .  $n$  is the number of atoms transferred from the supercell to reservoirs in forming the defect cell and  $q$  is the charge state of the defect  $\alpha$ . We also include a correction based on the alignment of the averaged electrostatic potentials by core level lineup.

Equation (1) indicates that the formation energies of doped Eu depend on the elemental chemical potentials, i.e., growth conditions, sensitively. Under thermal equilibrium growth conditions, the allowable values of each element's chemical potential  $\mu$  are constrained. First, to avoid the formation of elemental substances, the chemical potentials are bounded by

$$\mu_{\text{Eu}} \leq 0, \mu_{\text{Sr}} \leq 0, \mu_{\text{O}} \leq 0, \mu_{\text{M}} \leq 0, \text{M} = (\text{Ti}, \text{Zr}, \text{Hf}), \quad (2)$$

where  $\mu = 0$  is defined as the energy of the most stable solid or gas phase of each element. Second, to maintain the stable

TABLE III. Calculated and experimental formation energies of metal oxides. Experimental formation energies are from Scientific Group Thermodata Europe (SGTE) Solid SUBstance database [38].

Compound	Calculated $\Delta H_f$ (eV/atom)	Experimental $\Delta H_f$ (eV/atom)
SrTiO <sub>3</sub> ( <i>I4/mcm</i> )	-3.623	-3.463
SrZrO <sub>3</sub> ( <i>Pnma</i> )	-3.763	-3.663
SrHfO <sub>3</sub> ( <i>Pnma</i> )	-3.834	-3.702
SrO ( <i>Fm-3m</i> )	-3.111	-3.063
SrO <sub>2</sub> ( <i>I4/mmm</i> )	-2.262	-2.188
EuO ( <i>Fm-3m</i> )	-3.156	-3.057
Eu <sub>2</sub> O <sub>3</sub> ( <i>Ia-3</i> )	-3.125	-3.437
TiO <sub>2</sub> ( <i>I41/amd</i> )	-3.505	-3.261
Ti <sub>2</sub> O <sub>3</sub> ( <i>R-3</i> )	-3.322	-3.153
Ti <sub>3</sub> O <sub>5</sub> ( <i>C2/m</i> )	-3.394	-3.186
ZrO <sub>2</sub> ( <i>P21/c</i> )	-3.936	-3.801
HfO <sub>2</sub> ( <i>I41/amd</i> )	-4.004	-3.854

phase of perovskites, the sum of the chemical potentials of their constituent elements must be equal to the formation energies of perovskites,

$$\mu_{\text{Sr}} + \mu_{\text{M}} + 3 \times \mu_{\text{O}} = \Delta H_f(\text{SrMO}_3), \quad \text{M} = (\text{Ti}, \text{Zr}, \text{Hf}). \quad (3)$$

Finally, to prevent the precipitation of secondary phases of metal oxides, chemical potentials are limited by

$$m \times \mu_{\text{Sr}} + n \times \mu_{\text{O}} \leq \Delta H_f(\text{Sr}_m\text{O}_n), \quad (4a)$$

$$m' \times \mu_{\text{Eu}} + n' \times \mu_{\text{O}} \leq \Delta H_f(\text{Eu}_{m'}\text{O}_{n'}), \quad (4b)$$

$$m'' \times \mu_{\text{M}} + n'' \times \mu_{\text{O}} \leq \Delta H_f(\text{M}_{m''}\text{O}_{n''}). \quad (4c)$$

We take into account the stable phases of metal oxides. The calculated formation energies of the compounds are compared with experimental values in Table III, which are in good agreement.

Based on the constraints of chemical potentials, we can compute the accessible regions for the equilibrium growth of perovskites, as highlighted in Fig. 2. Outside the shaded areas, the growth processes of pure perovskites are unstable,

and competing phases could form as we have labeled. The chemical potential of O can be decided by Eq. (3), so the points with a certain value of  $\mu_{\text{O}}$  form a line with slope of  $-1$ .  $\mu_{\text{O}}$  is closer to zero for the line far away from the origin, corresponding to the O-rich condition. Similarly, the line close to the origin corresponds to the O-poor condition.

Because Ti, Zr, and Hf are the elements in the IVB column of the periodic table, many properties of the three SrMO<sub>3</sub> perovskites are similar. Therefore, we take SrZrO<sub>3</sub> as the example to discuss the doping properties of Eu. In Fig. 3(a), we compare the calculated formation energies of Eu<sub>Sr</sub>, Eu<sub>Zr</sub>, and Eu<sub>i</sub> in SrZrO<sub>3</sub> under the different conditions corresponding to A, B, and C points in Fig. 2. Under the O-poor condition corresponding to the A point, we scan the Fermi level through the whole band gap of SrZrO<sub>3</sub>, and find that instead of the Eu<sub>Zr</sub> defects with inversion symmetry, Eu<sub>Sr</sub> emerges as the most stable defect of Eu in a large part of the band gaps of SrZrO<sub>3</sub>. This is not ideal for developing MD emission materials. Under the O-rich condition corresponding to the B point, the formation energy of Eu<sub>i</sub> is relatively high due to the large size of the Eu atom. This indicates that the concentration of Eu<sub>i</sub> would be low. We therefore neglect Eu<sub>i</sub> in the following discussion and only investigate the competition between the two substitutional sites, Eu<sub>Sr</sub> and Eu<sub>Zr</sub>. The valences of Sr and Zr in SrZrO<sub>3</sub> are +2 and +4 in perovskites, respectively. So, for Eu<sub>Sr</sub> with the charge states of +2, +1, and 0, it corresponds to +4, +3, and +2 valence states of Eu, respectively. Similarly, for the charge state of -2, -1, and 0 of Eu<sub>Zr</sub>, the valence of Eu should be +2, +3, and +4, respectively. Because of the large band gap, initially, carrier densities of the perovskites are relatively low, and the Fermi levels are close to the middle of the band gap. When a large amount of Eu is introduced into the perovskites under the O-rich condition, Eu prefers to occupy at Zr sites and a significant amount of holes can be formed and the Fermi level shifts down to the VBM. As the Fermi level reaches the crossing point of the formation energy curves of Eu<sub>Sr</sub> and Eu<sub>Zr</sub>, it will be pinned by the self-compensation effect [31]. As a result, most of the Eu atoms have a valence of +3, either in the Eu<sub>Sr</sub>(+1) charge state or in the Eu<sub>Zr</sub>(-1) charge state. We also include the C condition with the lowest value of  $\mu_{\text{Zr}} - \mu_{\text{Sr}}$  in the allowable region. Then the difference between formation energies of Eu<sub>Sr</sub> and Eu<sub>Zr</sub> is maximized. Although the Eu<sub>Zr</sub> curve is

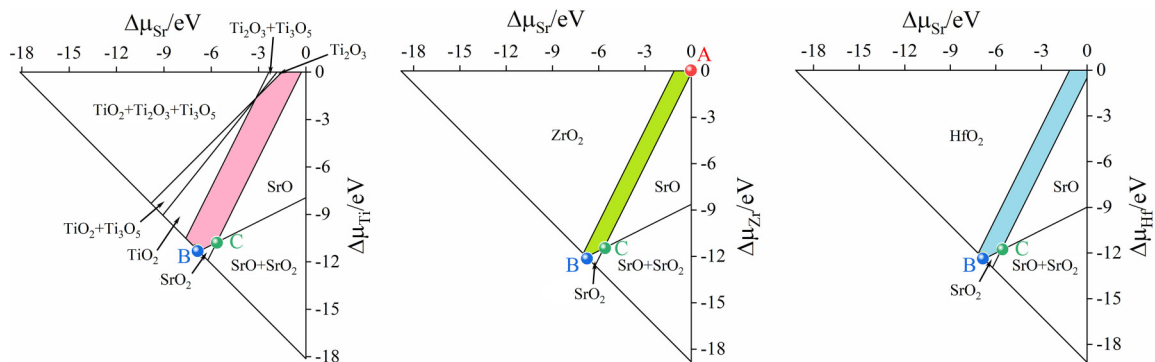


FIG. 2. Calculated stability diagrams of SrMO<sub>3</sub> ( $M = \text{Ti}, \text{Zr}, \text{Hf}$ ). The highlighted areas are the allowable chemical potential domain for the growth of SrMO<sub>3</sub>.

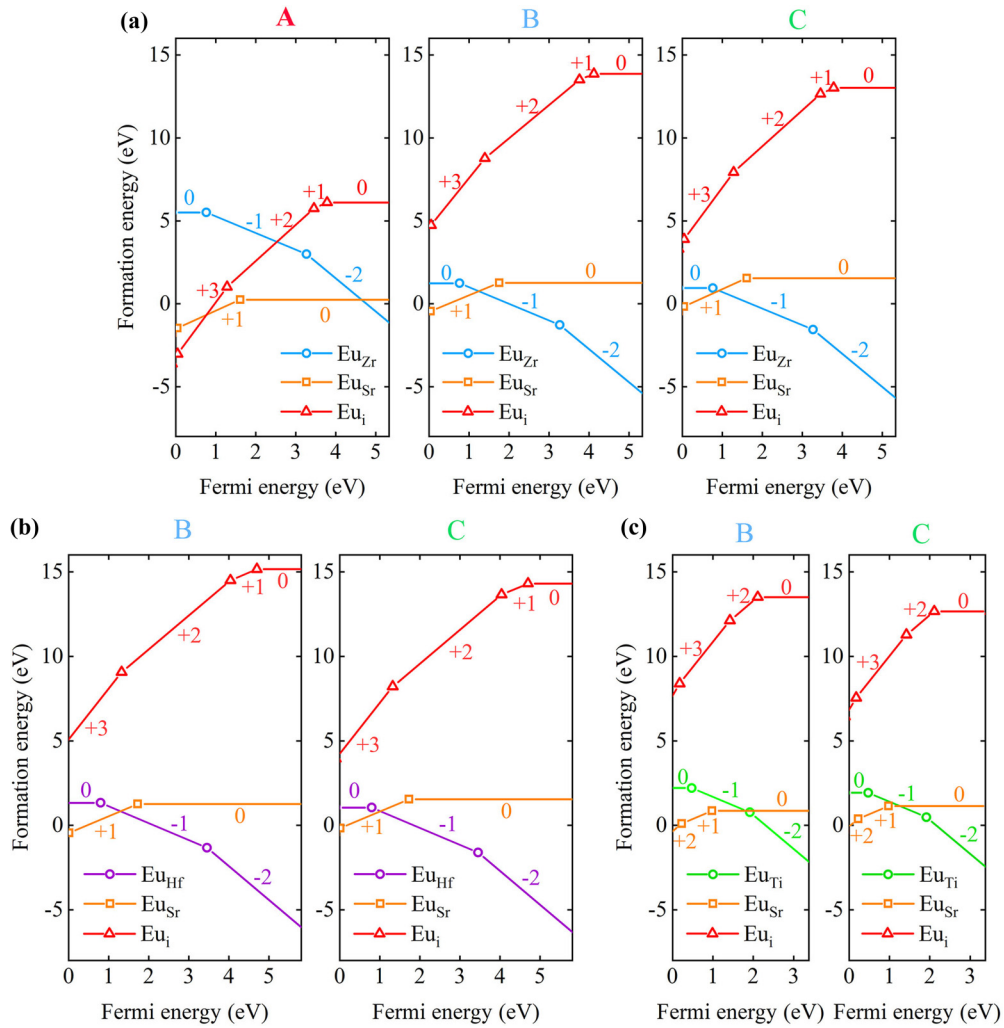


FIG. 3. (a) Formation energies of Eu in SrZrO<sub>3</sub> under conditions corresponding to A (O poor), B, and C (O rich) points in Fig. 2. (b), (c) Formation energies of Eu in SrHfO<sub>3</sub> and SrTiO<sub>3</sub> under B and C conditions.

lowered while Eu<sub>Sr</sub> curve is raised comparing with at condition B, the formation energies of the crossing point in C are the same as in B at about 0.753 eV. So, both the B and C are acceptable growth conditions for SrZrO<sub>3</sub>:Eu phosphor, and we will not include the O-poor condition in further discussion.

The doping property of Eu in SrHfO<sub>3</sub> is similar to that in SrZrO<sub>3</sub>. The crossing point of curves of Eu<sub>Sr</sub>(+1) and Eu<sub>Hf</sub>(-1) has a formation energy of 0.830 eV, as shown in Fig. 3(b). But Eu shows a different doping property in SrTiO<sub>3</sub>. In Fig. 3(c), under the B and C conditions as labeled in Fig. 2, the Fermi level is allowed between the Eu<sub>Sr</sub>(+1/0) transition level and the crossing point of Eu<sub>Sr</sub> and Eu<sub>Ti</sub> curves. Within this range, the Eu<sub>Sr</sub>(0) with +2 valence defects is relatively dominant. Considering that the formation energies of Eu<sub>Sr</sub>(+1) and Eu<sub>Ti</sub>(-1) are close to Eu<sub>Sr</sub>(0), the existence of Eu in +3 valence is also important. This is why Eu in both the +2 and +3 valences has been reported in SrTiO<sub>3</sub> experimentally [26,39]. Thus, SrTiO<sub>3</sub> is not an ideal host material for Eu<sup>3+</sup> phosphor.

For SrZrO<sub>3</sub> and SrHfO<sub>3</sub>, using the detailed balance equations [40], we find that under the O-rich growth conditions

of point B in Fig. 2, the Fermi level is already pinned at the crossing points of the formation energy curves of Eu<sub>Sr</sub> and Eu<sub>M</sub>, even for dopant density as low as 10<sup>6</sup>/cm<sup>3</sup>. At the crossing point, the concentrations of Eu<sub>Sr</sub>(+1) and Eu<sub>M</sub>(-1) are equal because they have the same formation energy. Therefore, simply increasing the concentration of Eu cannot effectively improve the ratio between Eu<sub>M</sub>(-1) and Eu<sub>Sr</sub>(+1) concentrations. This can be overcome by techniques such as applying strain during the growth of Eu-doped perovskites to suppress the donor defects Eu<sub>Sr</sub>(+1) and enhance the acceptor defect Eu<sub>M</sub>(-1), thus leading to a larger ratio of Eu<sub>M</sub>(-1) to Eu<sub>Sr</sub>(+1). When Eu substitutes Zr and Hf as Eu<sub>Zr</sub>(-1) and Eu<sub>Hf</sub>(-1), it would stretch the perovskite lattices. On the other hand, when Eu substitutes Sr as Eu<sub>Sr</sub>(+1), the lattices tend to shrink. So, tensile strain can lower the formation energy of Eu<sub>M</sub>(-1), while it raises that of Eu<sub>Sr</sub>(+1) [41]. To prove this, we calculate the formation energy difference of Eu<sub>Zr</sub>(-1) and Eu<sub>Sr</sub>(+1) under biaxial strain, as shown in Fig. 4. Thus, applying biaxial tensile strain during growth could effectively increase the concentration of Eu<sub>M</sub>(-1) and suppress the formation of Eu<sub>Sr</sub>(+1) in SrZrO<sub>3</sub> and SrHfO<sub>3</sub>.

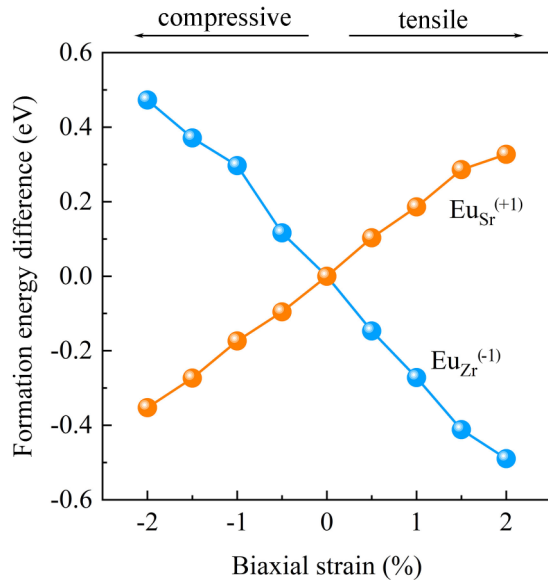


FIG. 4. Formation energy difference versus biaxial strain for  $\text{Eu}_{\text{Sr}}(+1)$  and  $\text{Eu}_{\text{Zr}}(-1)$  in  $\text{SrZrO}_3$ .

Moreover, raising the growth temperature and then quenching it to a working temperature could be another effective way to increase the concentration of  $\text{Eu}_{\text{M}}(-1)$  and suppress the formation of  $\text{Eu}_{\text{Sr}}(+1)$  in  $\text{SrZrO}_3$  and  $\text{SrHfO}_3$ . This is because at high growth temperature, high thermal excitation of electrons from valence bands to the conduction bands will push the Fermi level towards the center of the band gap. As shown in Fig. 3(a), under the oxygen rich condition, the formation energy of  $\text{Eu}_{\text{M}}(-1)$  is significantly lower than that of  $\text{Eu}_{\text{Sr}}(+1)$  when the Fermi level is close to the center of the band gap, so the defect concentration of  $\text{Eu}_{\text{M}}(-1)$  can be significantly enhanced compared to that of  $\text{Eu}_{\text{Sr}}(+1)$  when it is grown at high temperature and then quenched to a working temperature.

Finally, we estimate the emission energy of Eu in the perovskites. The electronic configuration of the  $\text{Eu}^{3+}$   $7F$  state has six spin-up  $f$  electrons, and the  $5D$  state that can be reached with one spin flip excitation has five spin-up and one spin-down  $f$  electrons, as shown in Fig. 5. Although the ground-state DFT calculation usually cannot deal with the excited state, the energy difference of  $7F_0$  and  $5D_0$  states can be calculated with relatively good accuracy as the energy difference of the high spin state of  $7F_0$  with  $6\mu_B$  and the low spin state of  $5D_0$  with  $4\mu_B$ , because of the localized nature of these states and error cancellation. The  $5D_0 \rightarrow 7F_0$  emission energy,  $\Delta E[\text{Eu}_{\text{M}}^{\text{em}}(-1)] =$

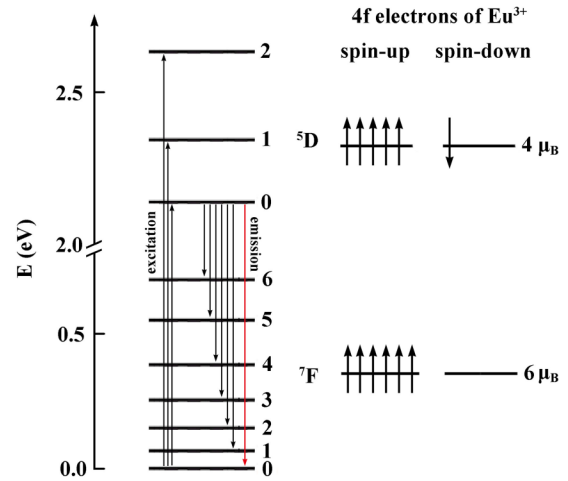


FIG. 5. Emission mechanism and 4f electron occupancy of  $\text{Eu}^{3+}$ .

$E[\text{Eu}_{\text{M}}(-1)|4\mu_B] - E[\text{Eu}_{\text{M}}(-1)|6\mu_B]$ , is labeled as the red arrow in Fig. 5, which is calculated to be 1.922, 2.195, and 2.130 eV in  $\text{SrTiO}_3$ ,  $\text{SrZrO}_3$ , and  $\text{SrHfO}_3$ , respectively, and is close to the experimental value of 2.138 eV (580 nm) [17].

#### IV. CONCLUSION

In summary, we have systematically investigated the doping properties of Eu in  $\text{SrTiO}_3$ ,  $\text{SrZrO}_3$ , and  $\text{SrHfO}_3$  using first-principles calculations. We have illustrated the desired growth conditions of Eu, obtained the formation energies of Eu impurities under different growth conditions, and provided various approaches to control the doping. We have explained the  $p$ -type dopability of Eu and the +3 valence state of Eu in both substitutional sites in  $\text{SrZrO}_3$  and  $\text{SrHfO}_3$ . The calculated emission energies of  $\text{Eu}^{3+}$  are in good agreement with experiment value. Our results provide a guideline for improving the  $5D_0 \rightarrow 7F_1$  MD emission in  $\text{Eu}^{3+}$ -doped perovskites, which could be beneficial for optomagnetism related applications.

#### ACKNOWLEDGMENTS

This work was supported by a CAEP Innovation Grant, PRC China (Grant No. CX20200011) and the Science Challenge Program (Grant No. TZ2016003-1). Z.-H.Y., S.S., and S.-H.W. were also supported by the National Natural Science Foundation of China (Grants No. 11804314, No. 62005256, No. 11634003, and No. U1930402). The National Supercomputer Center in Tianjin is acknowledged for computational support.

- [1] D. Wu, A. C. Sedgwick, T. Gunnlaugsson, E. U. Akkaya, J. Y. Yoon, and T. D. James, *Chem. Soc. Rev.* **46**, 7105 (2017).
- [2] C. K. Li, C. F. Kuang, and X. Liu, *ACS Nano* **12**, 4081 (2018).
- [3] A. M. Dibos, M. Raha, C. M. Phenicie, and J. D. Thompson, *Phys. Rev. Lett.* **120**, 243601 (2018).

- [4] L. D. Landau and E. Lifshitz, *Electrodynamics of Continuous Media* (Pergamon Press, Oxford, New York, Beijing, Frankfurt, 1984).
- [5] S. Freed and S. I. Weissman, *Phys. Rev.* **60**, 440 (1941).
- [6] C. M. Dodson and R. Zia, *Phys. Rev. B* **86**, 125102 (2012).
- [7] B. R. Judd, *Phys. Rev.* **127**, 750 (1962).

- [8] G. S. Ofelt, *J. Chem. Phys.* **37**, 511 (1962).
- [9] W. T. Carnall, P. R. Fields, and K. Rajnak, *J. Chem. Phys.* **49**, 4412 (1968).
- [10] W. T. Carnall, P. R. Fields, and B. G. Wybourne, *J. Chem. Phys.* **42**, 3797 (1965).
- [11] H. Giessen and R. Vogelgesang, *Science* **326**, 529 (2009).
- [12] A. Vaskin, S. Mashhadi, M. Steinert, K. E. Ching, D. Keene, S. Nanz, A. Abass, E. Rusak, D. Y. Choi, I. Fernandez-Corbaton, T. Pertsch, C. Rockstuhl, M. A. Noginov, Y. S. Kivshar, D. N. Neshev, N. Noginova, and I. Staude, *Nano Lett.* **19**, 1015 (2019).
- [13] M. Kasperczyk, S. Person, D. Ananias, L. D. Carlos, and L. Novotny, *Phys. Rev. Lett.* **114**, 163903 (2015).
- [14] Z. Q. Bian, K. Z. Wang, and L. P. Jin, *Polyhedron* **21**, 313 (2002).
- [15] Z. L. Fu, H. K. Yang, B. K. Moon, B. C. Choi, and J. H. Jeong, *Cryst. Growth Des.* **9**, 616 (2009).
- [16] A. K. Kunti, N. Patra, R. A. Harris, S. K. Sharma, D. Bhattacharyya, S. N. Jha, and H. C. Swart, *Inorg. Chem.* **58**, 3073 (2019).
- [17] S. M. Rafiaei, *Mater. Sci.-Poland* **34**, 780 (2016).
- [18] Y. Li, X. P. Gao, G. R. Li, G. L. Pan, T. Y. Yan, and H. Y. Zhu, *J. Phys. Chem. C* **113**, 4386 (2009).
- [19] H. Zhang, X. Fu, S. Niu, and Q. Xin, *J. Alloy. Compd.* **459**, 103 (2008).
- [20] Z. Lu, L. Chen, Y. Tang, and Y. Li, *J. Alloy. Compd.* **387**, L1 (2005).
- [21] G. Kresse and J. Furthmüller, *Phys. Rev. B* **54**, 11169 (1996).
- [22] P. E. Blöchl, *Phys. Rev. B* **50**, 17953 (1994).
- [23] J. Sun, A. Ruzsinszky, and J. P. Perdew, *Phys. Rev. Lett.* **115**, 036402 (2015).
- [24] J. Sun, R. C. Remsing, Y. Zhang, Z. Sun, A. Ruzsinszky, H. Peng, Z. Yang, A. Paul, U. Waghmare, X. Wu, M. L. Klein, and J. P. Perdew, *Nat. Chem.* **8**, 831 (2016).
- [25] J. Heyd, G. E. Scuseria, and M. Ernzerhof, *J. Chem. Phys.* **118**, 8207 (2003).
- [26] Y. G. Abreu, J. C. Soares, R. L. Moreira, and A. Dias, *J. Phys. Chem. C* **120**, 16960 (2016).
- [27] T. Matsuda, S. Yamanaka, K. Kurosaki, and S. Kobayashi, *J. Alloy. Compd.* **351**, 43 (2003).
- [28] A. Feteira, D. C. Sinclair, K. Z. Rajab, and M. T. Lanagan, *J. Amer. Ceram. Soc.* **91**, 893 (2008).
- [29] K. Tsuda and M. Tanaka, *Acta Crystallogr., Sect. A* **51**, 7 (1995).
- [30] L. S. Cavalcante, A. Z. Simoes, E. Longo, J. C. Sczancoski, R. Erlo, M. T. Escote, V. M. Longo, and J. A. Varela, *Solid State Sci.* **9**, 1020 (2007).
- [31] B. J. Kennedy, C. J. Howard, and B. C. Chakoumakos, *Phys. Rev. B* **60**, 2972 (1999).
- [32] K. van Benthem, C. Elsasser, and R. H. French, *J. Appl. Phys.* **90**, 6156 (2001).
- [33] Y. S. Lee, J. S. Lee, T. W. Noh, D. Y. Byun, K. S. Yoo, K. Yamaura, and E. Takayama-Muromachi, *Phys. Rev. B* **67**, 113101 (2003).
- [34] M. Sousa, C. Rossel, C. Marchiori, H. Siegwart, D. Caimi, J. P. Locquet, D. J. Webb, R. Germann, J. Fompeyrine, K. Babich, J. W. Seo, and C. Dieker, *J. Appl. Phys.* **102**, 104103 (2007).
- [35] P. Yang, B. Tai, W. Wu, J.-M. Zhang, F. Wang, S. Guan, W. Guo, Y. Lu, and S. A. Yang, *Phys. Chem. Chem. Phys.* **19**, 16189 (2017).
- [36] G. Pilania, S. K. Yadav, M. Nikl, B. P. Uberuaga, and C. R. Stanek, *Phys. Rev. Appl.* **10**, 024026 (2018).
- [37] S.-H. Wei and S. B. Zhang, *Phys. Rev. B* **66**, 155211 (2002).
- [38] Scientific Group Thermodata Europe, *Thermodynamic Properties of Inorganic Materials*, Vol. 19 (Springer-Verlag, Berlin, Heidelberg, 1999).
- [39] S. Katyayan and S. Agrawal, *J. Mater. Sci. Mater. Electron.* **30**, 10660 (2019).
- [40] J.-H. Yang, W.-J. Yin, J.-S. Park, J. Burst, W. K. Metzger, T. Gessert, T. Barnes, and S.-H. Wei, *J. Appl. Phys.* **118**, 025102 (2015).
- [41] J. Zhu, F. Liu, G. B. Stringfellow, and S.-H. Wei, *Phys. Rev. Lett.* **105**, 195503 (2010).